Numerical Study of an Ultra-Broadband and Wide-Angle Insensitive Perfect Metamaterial Absorber in the UV–NIR Region

Thi Quynh Mai Nguyen[1] · Thi Kim Thu Nguyen[1,4] · Dac Tuyen Le[2] · Chi Lam Truong[3] · Dinh Lam Vu[4] · Thi Quynh Hoa Nguyen[1] ⬤

Abstract

Developing a simple structure using low-cost material that enables both large-scale fabrication and broadband absorption response is highly desirable but very challenging for achieving high-performance metamaterial absorber. Herein, we propose and numerically investigate an ultra-broadband and wide-angle insensitive perfect metamaterial absorber in the ultraviolet to near-infrared (UV–NIR) region based on a simple metal–dielectric–metal structure. The proposed absorber structure consists of a periodic array of a tungsten hexagonal prism and a tungsten ground plane separated by a silicon dioxide dielectric substrate. The proposed absorber achieves an ultra-broadband absorption response in the range of 275–1000 nm with an absorptivity above 90% and a relative bandwidth of 106.8% at normal incidence, which covers from the UV to NIR region. The absorption efficiency is maintained with the figure of merit η_{OBW} higher than 90% for a wide incident angle up to 40° for transverse electric (TE) polarization and 65° for transverse magnetic (TM) polarization. The effects of structural parameters and different metallic materials on the absorption performance are presented. In addition, the physical mechanism is analyzed using the surface density and distributions of electric and magnetic fields that are attributed to both localized surface plasmon (LSP) and propagating surface plasmon (PSP) resonances. Owing to outstanding merits of simple structure, low cost, and high absorption performance, the designed absorber can be suitable for many applications in the UV–NIR spectrum such as thermal emitters and solar cells.

Keywords Metamaterials · Absorber · UV–NIR · Broadband · Surface plasmon resonance

Introduction

Metamaterial absorber (MA) is a fast-growing field with various potential applications like sensors [1–3], thermal emitters [4, 5], and solar cells [6–8], since Landy et al. first proposed a nearly perfect absorber in 2008 [9]. The MA usually operates at a specific frequency and has a narrow bandwidth owing to its resonance nature. Therefore, many design approaches have been developed to extend the bandwidth of MAs such as using fractal structures [10–12], loading with lumped devices [13–15], and multilayer metal–dielectric stacks [16–23]. However, these approaches remain a significant limit in design and/or fabrication regards costly and time-consuming. Recently, the simple design of broadband MA structures based on a single stack of metal–dielectric–metal configuration has been proposed, but most of the these studies only focused on visible (VIS) [12, 24, 25], VIS to near-infrared (NIR) [26–28], and UV–VIS region [29]. Therefore, the MA design that can extend the absorption band from the UV into the infrared (IR) region to efficiently absorb the solar radiation energy has been demonstrated. For instance, Huang et al. proposed the metamaterial perfect absorber, which consists of a periodic array of tungsten (W) cylinders covered by a silicon carbide (SiC) layer and a silicon dioxide (SiO_2) layer and exhibits an efficient ultra-broadband absorption from UV to NIR (200–900 nm)

✉ Thi Quynh Hoa Nguyen
  ntqhoa@vinhuni.edu.vn

1   School of Engineering and Technology, Vinh University, 182 Le Duan, Vinh, Vietnam

2   Department of Physics, Hanoi University of Mining and Geology, 18 Pho Vien, Hanoi 100000, Vietnam

3   NTT Hi-Tech Institute, Nguyen Tat Thanh University, Ho Chi Minh City, Vietnam

4   Graduate University of Science and Technology, Vietnam Academy of Science and Technology, 18 Hoang Quoc Viet, Hanoi, Cau Giay, Vietnam

[30]. Liu et al. designed the multilayer silicon/iron (Si/Fe) absorber with an average absorptivity of over 96% in the range of 300–3000 nm under the normal incident, which covers from the ultraviolet to mid-infrared (UV–MIR) region [28]. Even though these MA exhibited the ultra-broadband band and high absorption efficiency, their fabrication processes are complex. Therefore, the design of MA remains a significant challenge to achieve simultaneously simple structure for fabrication, low cost, high absorption efficiency and performance.

In this study, we propose a simple design of an ultra-broadband and wide-angle insensitive MA using a dielectric–metallic–dielectric structure operating in the UV–NIR region. The proposed MA is composed of a periodic array of a tungsten hexagonal prism and a silicon dioxide dielectric substrate backed with a tungsten ground plane. The designed absorber exhibits an ultra-broadband absorption response with an absorptivity than 90% in the range from 275 nm to 1000 nm and a relative bandwidth of 106.8% at normal incidence. Moreover, this design is realized for a wide incident angle and polarization insensitivity. The effects of structural parameters and different metallic materials on absorption performance and the physical mechanism of the proposed MA are numerically investigated in detail in the following sections.

Structure Design and Method

Figure 1 illustrates a schematic of the proposed ultra-broadband MA. The designed MA structure is composed of a two-dimensional periodic arrangement of unit cells along x- and y- axes (Fig. 1a). The unit cell consists of a metallic hexagonal prism placed on the top of a dielectric substrate with a metallic ground plane, as shown in Fig. 1b. Both the metallic layers of the unit cell is made by tungsten (W). The hexagonal prism has a prism base edge (R) of 100 nm and a prism height (t_m) of 50 nm. The unit cell has a period constant (P) of 290 nm. The dielectric substrate is made by silicon dioxide (SiO_2) with thickness (d) of 40 nm. The thickness of the continuous bottom layer (t_d) is chosen to be 150 nm to blocked the transmission of the incident light. The thickness of the metallic ground layer is usually chosen in such a way that it is greater than the skin depth of the incident light. The dielectric constants of tungsten are taken from Palik [31], while silicon dioxide from Ghosh [32].

To investigate the performance of the designed ultra-broadband MA structure, we use the commercial computer simulation technology (CST) Microwave Studio software with a frequency-domain solver. In the simulation setup, the periodic boundary conditions are assigned to unit cell for the x and y directions, and the open boundary condition is fixed to the z-direction. The simulation is performed in free space.

The absorption ($A(\omega)$) of a MA is calculated as Eq. (1).

$$A(\omega) = 1 - R(\omega) - T(\omega) = 1 - \left|S_{11}(\omega)\right|^2 - \left|S_{12}(\omega)\right|^2 \quad (1)$$

where, $R(\omega)$ and $T(\omega)$ are frequency-dependent transmission and reflection coefficients, which are determined from the frequency-dependent S-parameters $S_{11}(\omega)$ and $S_{12}(\omega)$ with $R(\omega)=\left|S_{11}(\omega)\right|^2$ and $T(\omega)=\left|S_{12}(\omega)\right|^2$. Due to the continuous metallic covering on the bottom layer of the MA structure, the transmission of EM wave is blocked ($T(\omega) = 0$). Therefore absorption is simply defined as Eq. (2).

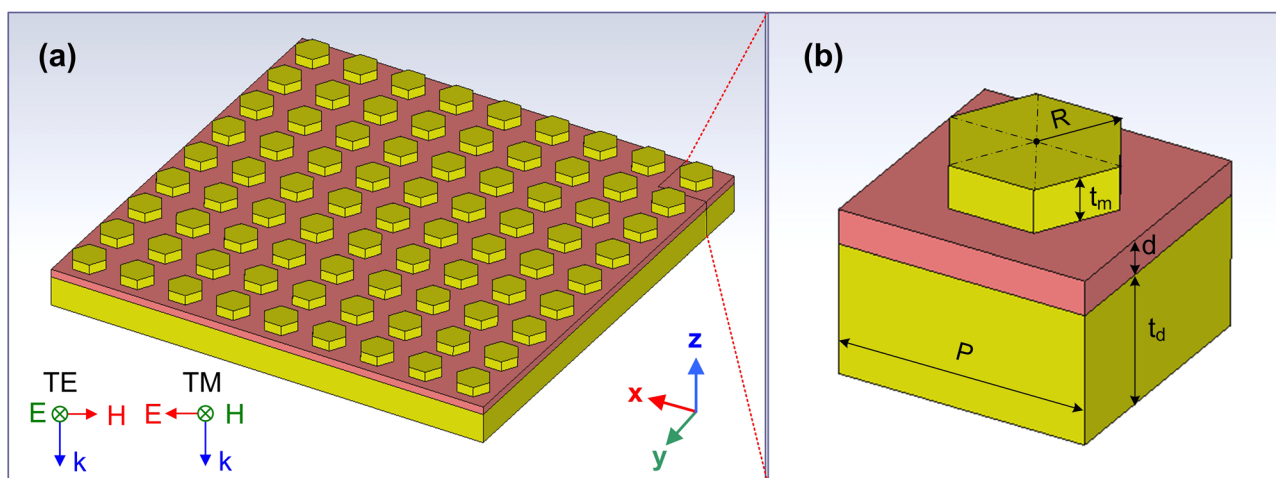$$A(\omega) = 1 - \left|S_{11}(\omega)\right|^2 \quad (2)$$

Fig. 1 (a) Schematic of the proposed ultra-broadband MA and (b) Magnified 3-D view unit cell of the MA

The wideband absorption characteristic of a MA can be evaluated from the relative absorption bandwidth (*RBW*) defined as Eq. (3).

$$RBW = 2 \times \frac{f_U - f_L}{f_U + f_L},$$
(3)

where f_U and f_L are the upper and lower limits of a wavelength range with the absorptivity above 90%.

Results and Discussion

a. Absorption performance at normal incidence and oblique incidence

Figure 2 shows the absorption, reflection, and transmission spectra of the proposed MA at normal incidence. The $T(\omega)$ is plotted on the right axis and it is nearly zero in the entire simulation range of 250-1250 nm. The $R(\omega)$ yields a value of below 0.1 in the range of 275-1000 nm, as plotted in the left axis in Fig. 2. Therefore, the proposed MA structure achieves an ultra-broadband absorption response with the absorptivity above 90% ranging from 275 nm to 1000 nm, which covers from UV to the NIR region. Furthermore, three district absorption peaks can be observed at 286 nm, 400 nm, and 750 nm with the corresponding absorptivity of 0.96, 0.98, and 0.98, respectively. The proposed MA achieves the *RBW* value of 106.8%, which proves an ultra-broadband absorption characteristic.

For practical applications, the absorber structure need maintain its absorption performance with a wide incident angle due to the fact that the electromagnetic (EM) wave is obliquely incident onto the surface of the absorber structure.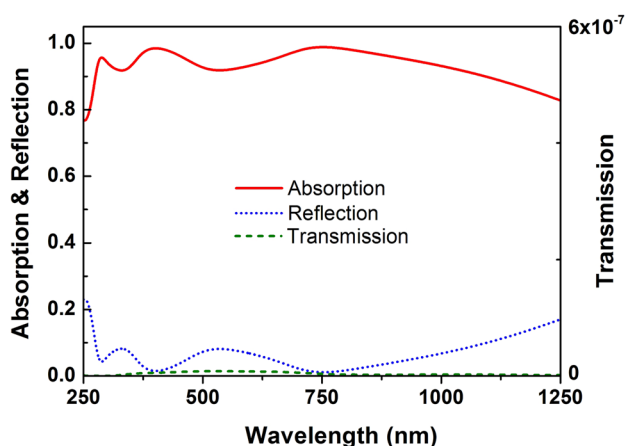 The reflection coefficients for the TE polarization ($\Gamma_\perp$) and the TM polarization ($\Gamma_\parallel$) under the oblique incidence angle are defined by Eqs. (4) and (5) [12, 25, 33].

$$\Gamma_\perp = \frac{Z_m cos\theta_i - Z_0 cos\theta_t}{Z_m cos\theta_i + Z_0 cos\theta_t}$$
(4)

$$\Gamma_\parallel = \frac{Z_m cos\theta_t - Z_0 cos\theta_i}{Z_m cos\theta_t + Z_0 cos\theta_i}$$
(5)

where θ_i and θ_t are the incidence and transmission angle, respectively. From Eqs. (4) and (5), it indicates that the reflection coefficient changes with varying the incident angle. It means that the absorption coefficient of MA also depends on the incident angle. To prove that the absorption spectra of the proposed MA with various the incident angle for TE and TM polarizations are investigated as shown in Fig. 3. The incident angle is varied in the range of 0-80° with a step size of 5°. As seen in Fig. 3, it is found that the absorptivity is decreased with increasing the incidence angle for both TE and TM polarizations. However, the absorptivity is still more than 80% with incidence angle up to 45° and 70° in the whole wavelength range of 275–1000 nm for TE and TM polarizations, respectively. It indicates that the proposed MA has a wide-angle characteristic.

To further analyze the performance characteristics of the proposed MA, the figure of merit (FOM) and operational bandwidth (OBW) is evaluated. The FOM (η_{OBW}) can be related to *OBW* as Eq. (6) [17, 25].

$$\eta_{OBW} = \frac{1}{\lambda_U - \lambda_L} \int_{\lambda_U}^{\lambda_U} A(\lambda)d\lambda = \frac{1}{OBW} \int_{\lambda_U}^{\lambda_U} A(\lambda)d\lambda$$
(6)

In this proposed MA, the operation wavelength is determined in the fixed range of 275–1000 nm, which is equal to the OBW of 725 nm. The plots of (η_{OBW}) as a function of the incident angles for TE and TM polarizations as presented in Fig. 4. The η_{OBW} is 0.957 at normal incidence, and decreases slightly to 0.926 for TE polarization and 0.952 for TM polarization at incident angle of 30°. The η_{OBW} remains above 0.9 with incidence up to 40° and 65° and 0.8 with incidence up to 55° and 79° for TE and TM polarizations, respectively.

Furthermore, the dependence of absorption spectra on the polarization angles in the range of 0–90° with a step size of 15° under normal incidence is simulated as shown in Fig. 5. Under both TE and TM polarizations, with increasing the polarization angle from 0° to 90° for the normal incident angle, the ultra-broadband perfect absorption response (above 90%) is unchanged in the entire wavelength band. It confirms that the proposed MA shows polarization-insensitive characteristics due to its symmetry structure.
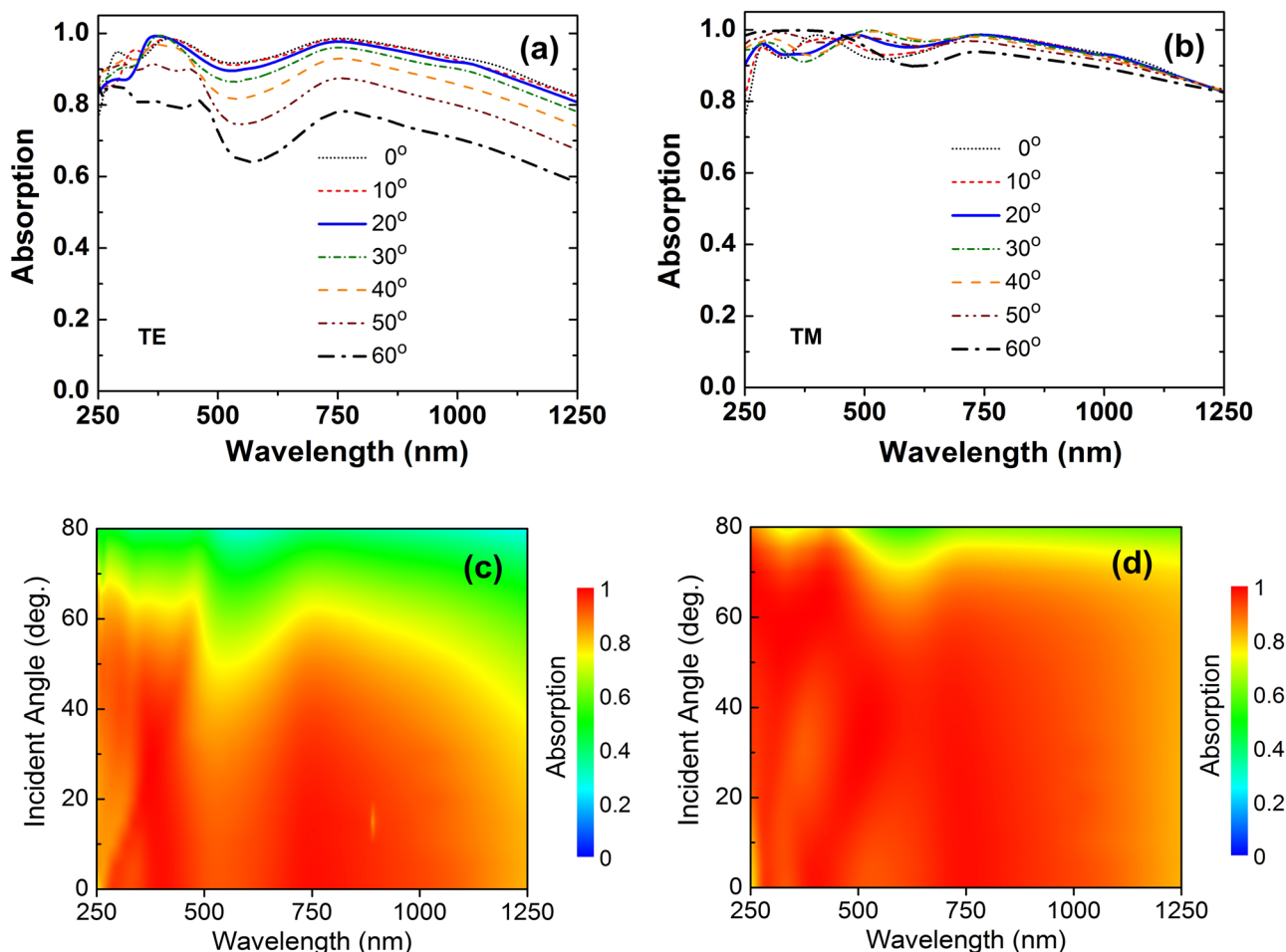

Fig. 2 Absorption, reflection, and transmission spectra of the proposed ultra-broadband MA

Fig. 3 The selected absorption spectra and absorption map of the proposed MA with various incident angles for **(a, c)** TE and **(b, d)** TM polarizations, respectively

b. Absorption Mechanism

The impedance matching is a prerequisite to exhibit a resonant behavior. When the impedance of MA (Z_m) and the impedance of free-space (Z_0) are matched, the reflection coefficient (Γ), defined as Eq. (7), becomes zero to realize

Fig. 4 The η_{OBW} of the proposed MA with various incident angles for TE and TM polarizations

the perfect absorbance. Ideally, the MA impedance can be controlled by the permeability (μ_m) and permittivity (ϵ_m) of medium. The effective impedance (Z_{eff}) can be extracted using scattering parameters from Eq. (8) [24, 25, 33, 34].

$$\Gamma = \frac{Z_m - Z_0}{Z_m + Z_0} \quad \text{with} \quad Z_m = Z_0 \sqrt{\frac{\mu_m}{\epsilon_m}} \tag{7}$$

$$Z_{eff} = \frac{Z_m}{Z_0} = \sqrt{\frac{(1 + S_{11})^2 - S_{12}^2}{(1 - S_{11})^2 - S_{12}^2}} = \frac{1 + S_{11}}{1 - S_{11}} \tag{8}$$

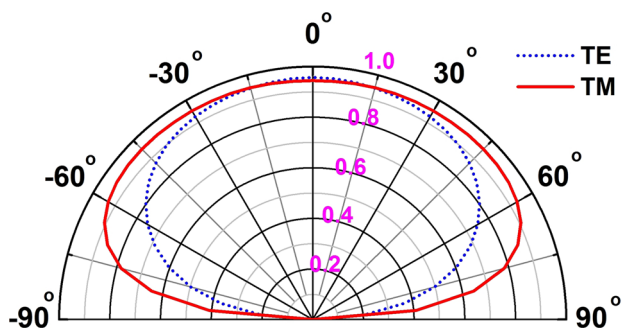Figure 6 shows the retrieved effective impedance (Z_{eff}) of proposed MA which consists of the real and imaginary part of (Z_{eff}). As seen in Fig. 6, the real and imaginary part becomes unity and zero at the wavelength range of 275 nm to 1000 nm, respectively, which confirms the impedance matching and the presence of perfect ultra-broadband absorption.
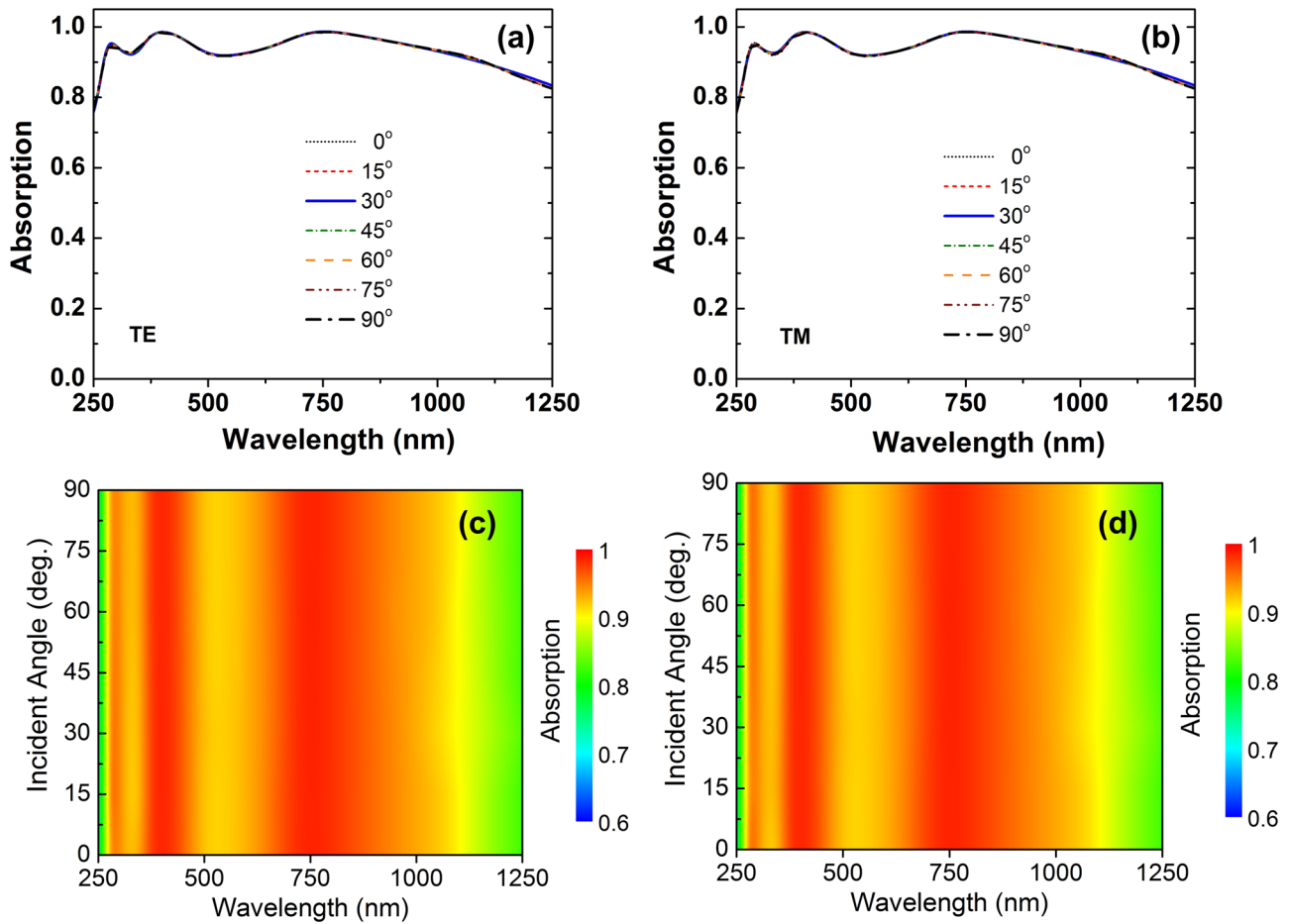
Fig. 5 The selected absorption spectra and absorption map of the proposed MA with various polarization angles under (**a**, **c**) TE and (**b**, **d**) TM polarizations, respectively

To further investigate the physical mechanism, we have simulated the current density, distributions of the electric field, and magnetic field of the proposed MA at the various
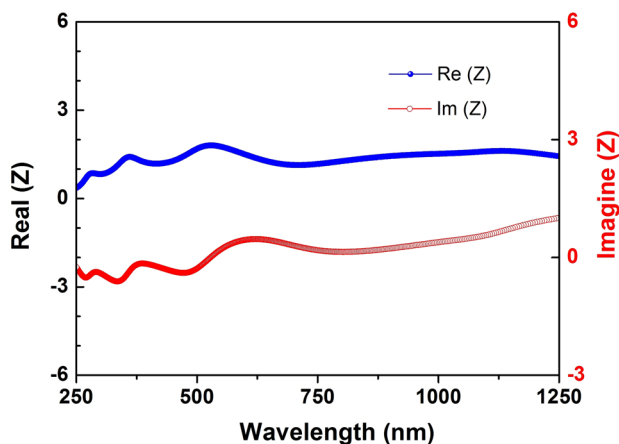

Fig. 6 Normalized impedance of the proposed MA under normal incidence

resonant wavelengths of 286 nm, 400 nm, and 750 nm in the YOZ plane for TE polarization as presented in Fig. 7. It is clear from Fig. 7a–c, the current density accumulates in the top and bottom metal layers which affirms the presence of the surface plasmon resonance (SPR) [24]. It was reported that the electric current concentrates only on both metallic layers sandwiched by a dielectric layer that means the origins of the energy loss in the dielectric layer which results in the broadband absorption [26]. From the distribution of electric field at various wavelengths 286 nm, 400 nm, and 750 nm as shown in Fig. 7d–f, It is clear that the light is coupled to the edge of the W prism and localized in the air-gap of the adjacent W prism. This indicates that the surface plasmon polaritons (SPPs) are excited in the metamaterial absorber [26, 28]. Meanwhile, there is an intrinsic difference in the magnetic field distributions of the resonant wavelengths as seen in Fig. 7g–k. At the short resonant wavelength of 286 nm, the magnetic field is not only intensively concentrated in the metallic corners of the adjacent W prism, but also distributed between

Fig. 7 **(a–c)** Current density, **(d–f)** electric field distribution on the XOY plane, and **(g, h, k)** magnetic field distribution on the XOZ plane of a unit cell of the proposed absorber under normal incidence at various resonant wavelengths of 286 nm, 400 nm, and 750 nm, respectively. The x- and y-directions are taken form –145 nm to 145 nm
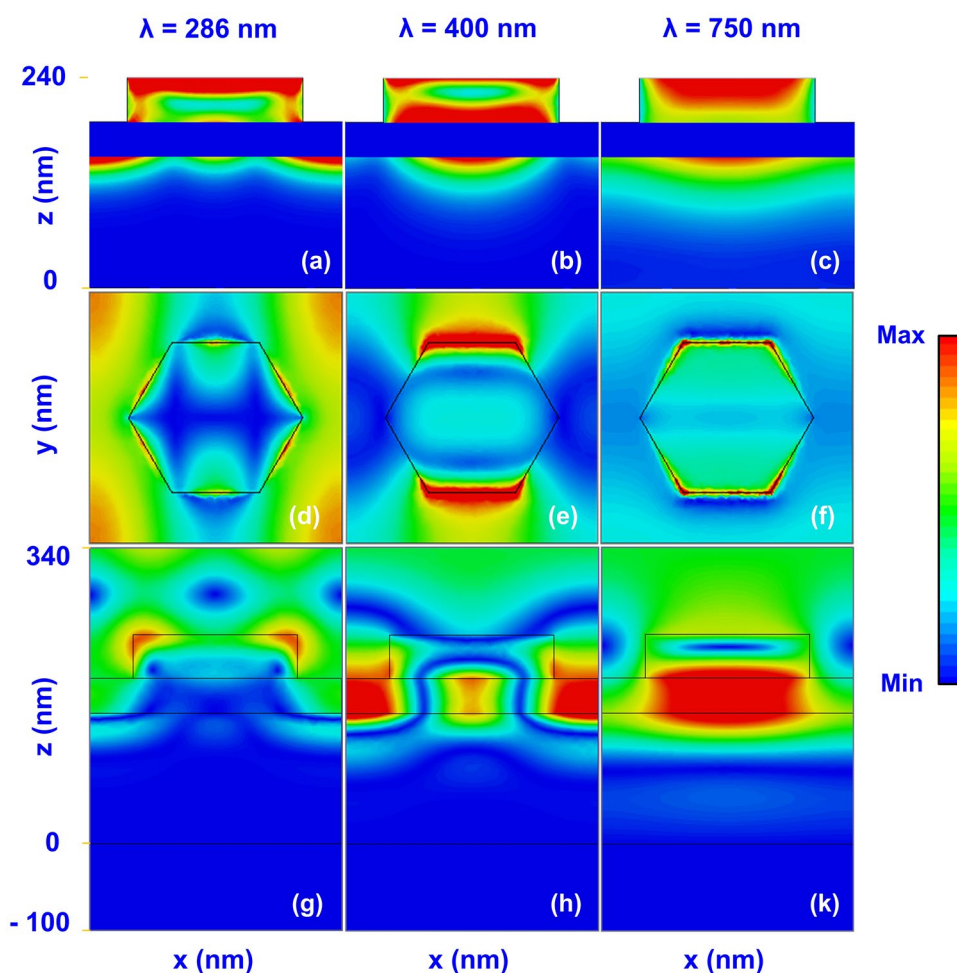
the adjacent cells (Fig. 7g). Thus, the perfect absorption at this resonant wavelength is caused by the excitation of a propagating surface plasmon (PSP) resonance. At a longer resonant wavelength of 750 nm, the magnetic field is confined within the gap between the W prism and the W ground plane (Fig. 7k). It means that the localized surface plasmon (LSP) resonance is contributed to the resonance wavelength of 750 nm. Finally, at resonant wavelength of 400 nm, it can be seen that electric field is not only mainly confined within the gap between both metallic layers but also appeared in the area between adjacent W prism (Fig. 7h), indicating that the perfect absorption in this resonant wavelength of 750 nm is due to the combinations of the PSP and LSP resonances.

c. Parametric Analysis

We studied the effects of different structure parameters on the absorption spectra and the corresponding η_{OBW} of the proposed MA as shown in Figs. 8 and 9,

respectively. The η_{OBW} is calculated in the wavelength range from 275 to 1000 nm. Based on this study, the optimized structure can be reached as shown in Fig. 1. Figures 8a and 9a show the variations of absorption spectrum and the corresponding η_{OBW} as a function of the thickness of dielectric layer (h) and the other parameters shown Fig. 1 are fixed. When h value increases from 30 nm to 60 nm, the absorption bandwidth and the η_{OBW} of the MA increases and reaches an optimum value at 40 nm, and then decreases as further increasing of the h value. The same trends can be observed in Figs. 8b and 9b by varying the periodic unit cell (P), that obtains optimum value at $P = 150$ nm. Figures 8c and 9c shows the variation in absorption performance caused by changing the prism height (t). The absorption bandwidth of the proposed MA increases with increasing the t value from 40 nm to 75 nm while the η_{OBW} first increases, reach an optimum value at 60 nm, and then decrease as the prism height (t) further increase. Meanwhile, the η_{OBW} of the proposed MA decreases with increasing the prism base
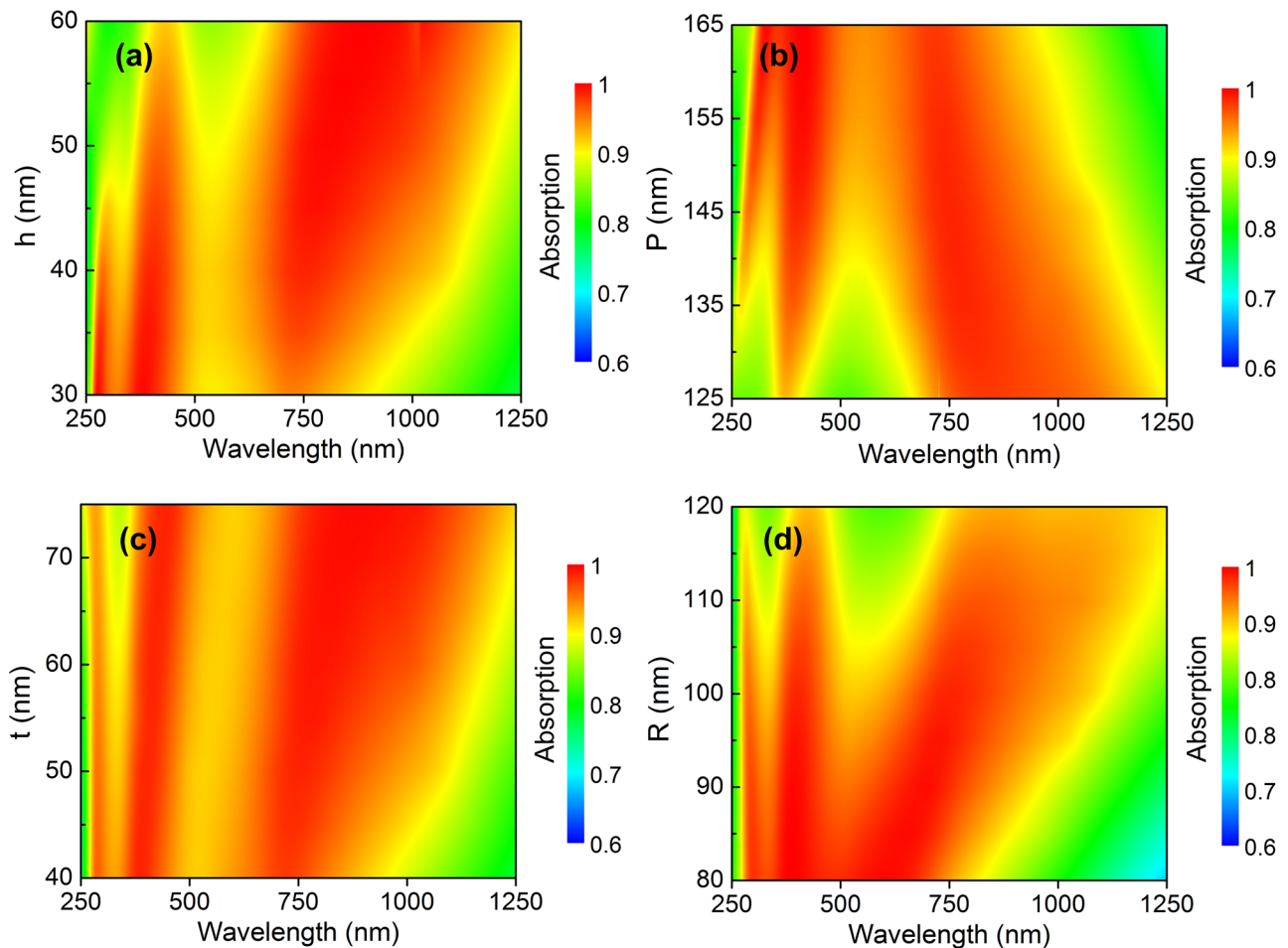
Fig. 8 Absorption spectra variations in various structural parameters for the proposed MA at the normal incidence: **(a)** thickness of dielectric layer (*h*), **(b)** periodic unit cell (*P*), **(c)** prism height (*t*), and **(d)** prism base edge (*R*)

edge (*R*) from 75 nm to 125 nm as shown in Fig. 9d. However, the proposed MA exhibits the largest absorption spectrum when the thickness of the *R* value is 100 nm as observed in Fig. 8d. The variations of the absorption spectra with changing the structural parameters can explain by the variations in the impedance of the MA. The input impedance of the MA changes with varying the structure parameters, leading to the changing of wavelength range that occurring the impedance matching, resulting in the changing of the perfect absorption response of the MA.

Finally, the effect of various metallic materials such as noble metal (Au) and cheap metals (Cu, Ni, W) on the absorption spectra of the proposed MA is analyzed, as depicted in Fig. 10. As shown in Fig. 10, the bandwidth of the proposed MA shrinks in the lower absorption wavelength region when Cu and Au are used as metallic layers of the designed structure. Meanwhile, with Ni-based MA, the absorption spectrum is extended to a longer absorption wavelength, but the absorptivity is significantly decreased in the range of 520–880 nm. This observation is caused by the intrinsic dispersion property of metallic materials [28]. The wavelength-dependent dispersion constant of W and Ni metals shows the relatively flat compared with that of Cu and Au metals in the wavelength in the range of 250-1000 nm, as proved in Fig. 11. Thus, both cheap metals of Ni and W can become a good candidate for the design of waveband MA operating in the UV–NIR region.
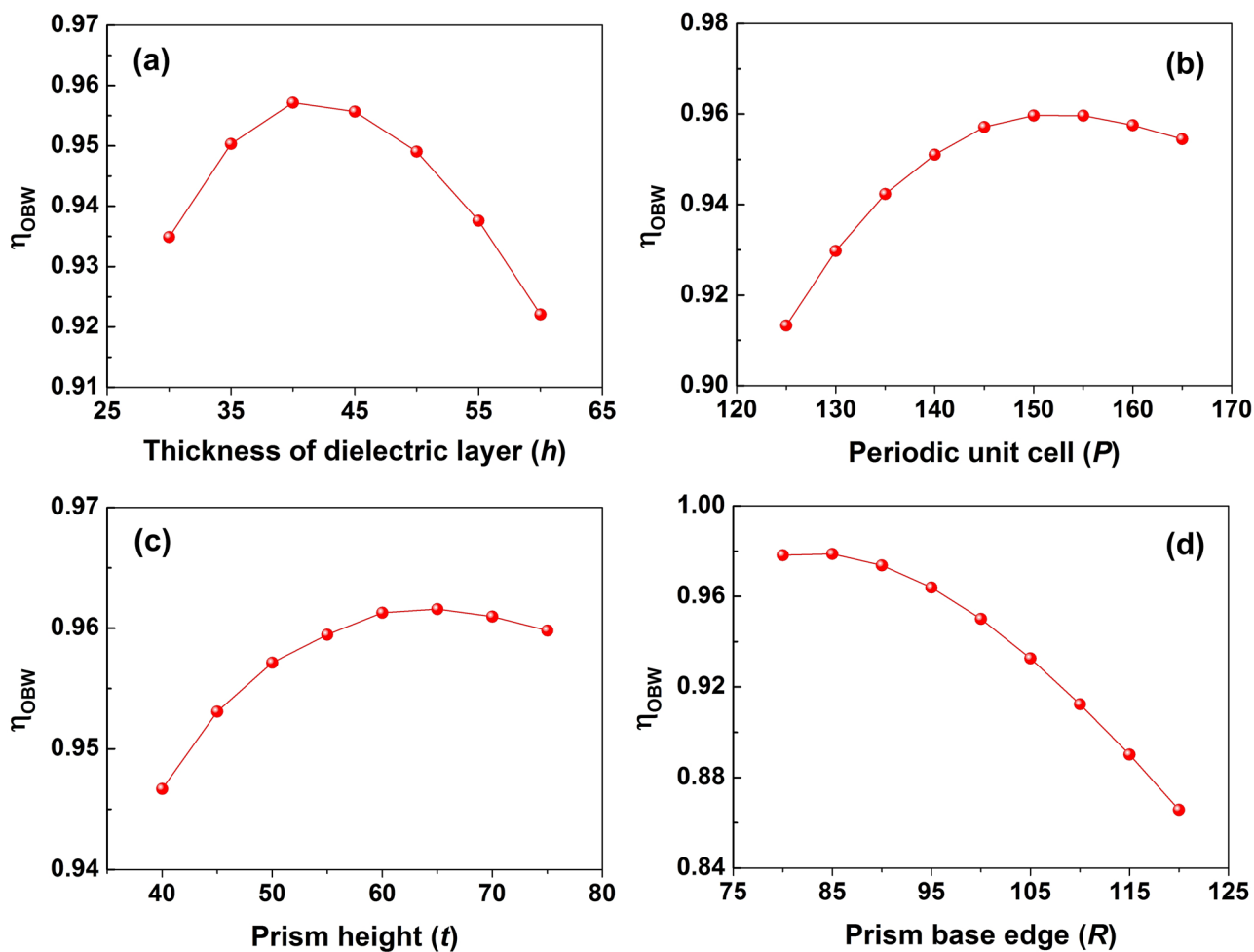
Fig. 9 The η_{OBW} variations in various structural parameters for the proposed MA at the normal incidence: (**a**) thickness of dielectric layer (h), (**b**) periodic unit cell (P), (**c**) prism height (t), and (**d**) prism base edge (R)
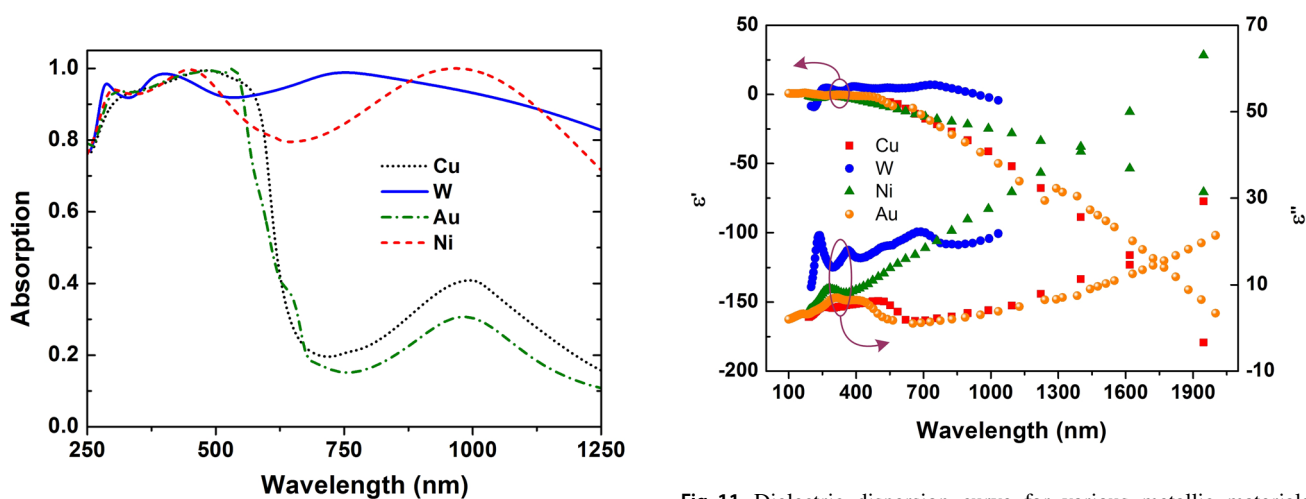

Fig. 10 Effect of metallic materials on the absorption spectra of the proposed MA under normal incidence

Fig. 11 Dielectric dispersion curve for various metallic materials, where ϵ' and ϵ'' is the real and imaginary part of dielectric dispersion, respectively. Refractive index database for W and Au from ref. [31], Ni from ref. [35], and Cu from ref. [36]

Conclusion

We have proposed and numerically investigated an ultra-broadband and wide-angle insensitive perfect metamaterial absorber in the UV–NIR region based on a metal–dielectric–metal structure. The proposed MA structure consists of a periodic array of a tungsten hexagonal prism and a silicon dioxide dielectric substrate backed with a tungsten ground plane. The proposed MA showed an ultra-broadband absorption in the range of 275-1000 nm with an absorptivity above 90%, OBW of 725 nm, and a relative bandwidth of 106.8% at normal incidence. The physical mechanism of the MA was revealed by the input impedance and the surface current density, and the distributions of electric and magnetic fields. Moreover, the effect of the structural parameters and different metallic materials on the absorption performance have been presented. The designed structure exhibited the insensitive polarization and ultra-broadband absorption response with η_{OBW} higher than 90% for a wide incident angle up to 40° for TE polarization and 65° for TM polarization. The designed structure is very simple, low cost, and good absorption performance, and thus it can be a good candidate for many applications in the UV–NIR spectrum such as thermal emitters and thermophotovoltaics.

Declarations

References

1. Luo S, Zhao J, Zuo D, Wang X (2016) Perfect narrow band absorber for sensing applications. Opt Express 24(9):9288. https://doi.org/10.1364/OE.24.009288

2. Abdulkarim YI, Deng L, Altntag O, Unal E, Karaaslan M (2019) Metamaterial absorber sensor design by incorporating swastika shaped resonator to determination of the liquid chemicals depending on electrical characteristics. Physica E 114:113593. https://doi.org/10.1016/j.physe.2019.113593

3. Liao YL, Zhao Y (2020) Ultra-narrowband dielectric metamaterial absorber with ultra-sparse nanowire grids for sensing applications. Sci Rep 10:1480. https://doi.org/10.1038/s41598-020-58456-y

4. Liu X, Tyler T, Starr T, Starr AF, Jokerst NM, Padilla WJ (2011) Taming the Blackbody with Infrared Metamaterials as Selective Thermal Emitters. Phys Rev Lett 107:045901. https://doi.org/10.1103/PhysRevLett.107.045901

5. Kong A, Cai B, Shi P, Yuan XC (2019) Ultra-broadband all-dielectric metamaterial thermal emitter for passive radiative cooling. Opt Express 27(12):30102–30115. https://doi.org/10.1364/OE.27.030102

6. Wang Y et al (2012) Metamaterial-plasmonic absorber structure for high efficiency amorphous silicon solar cells. Nano Lett 12:440–445. https://doi.org/10.1021/nl203763k

7. Hägglund C, Apell SP (2012) Plasmonic Near-Field Absorbers for Ultrathin Solar Cells. J Phys Chem Lett 3(10):1275–1285. https://doi.org/10.1021/jz300290d

8. Liu Y, Chen Y, Li J, Hung TC, Li J (2012) Study of energy absorption on solar cell using metamaterials. Sol Energy 86(5):1586–1599. https://doi.org/10.1103/PhysRevLett.100.207402

9. Landy NI, Sajuyigbe S, Mock JJ, Smith DR, Padilla WJ (2008) Perfect metamaterial absorber. Phys Rev Lett 100(20):207402. https://doi.org/10.1021/acsphotonics.7b00906

10. Kenney M, Grant J, Shah YD, Escorcia-Carranza I, Humphreys M, Cumming DRS (2017) Octave-spanning broadband absorption of terahertz light using metasurface fractal-cross absorbers. ACS Photonics 4(10):2604–2612. https://doi.org/10.1021/acsphotonics.7b00906

11. Kenney M, Grant J, Cumming DRS (2019) Alignment-insensitive bilayer THz metasurface absorbers exceeding 100% bandwidth. Opt Express 27(15):20886–20900. https://doi.org/10.1364/OE.27.020886

12. Bilal RMH, Saeed MA, Choudhury PK, Baqir MA, Kamal W, Ali MM, Rahim MM (2020) Elliptical metallic rings–shaped fractal metamaterial absorber in the visible regime. Sci Rep 10:14035. https://doi.org/10.1038/s41598-020-71032-8

13. Shang Y, Shen Z, and Xiao S (2013) On the design of single-layer circuit analog absorber using double-square-loop array. IEEE Trans Antennas Propag 61(12):6022–6029. https://doi.org/10.1109/TAP.2013.2280836

14. Nguyen TT, Lim S (2018) Design of metamaterial absorber using eight-resistive-arm cell for simultaneous broadband and wide-incidence-angle absorption. Sci Rep 8:6633. https://doi.org/10.1038/s41598-018-25074-8

15. Nguyen TQH, Nguyen TKT, Cao TN, Nguyen H, Bach LG (2020) Numerical study of a broadband metamaterial absorber using a single split circle ring and lumped resistors for X-band applications. AIP Adv 10:035326. https://doi.org/10.1063/1.5143915

16. Cui Y, Fung KH, Xu J, Ma H, Jin Y, He S, Fang NX (2012) Ultra-broadband light absorption by a sawtooth anisotropic metamaterial slab. Nano Lett 12(3):1443–1447. https://doi.org/10.1021/nl204118h

17. Lobet M, Lard M, Sarrazin M, Deparis O, Henrard L (2014) Plasmon hybridization in pyramidal metamaterials: a route towards ultra-broadband absorption. Opt Express 22:12678–13690. https://doi.org/10.1364/OE.22.012678

18. Lin Y, Cui Y, Ding F, Fung KH, Ji T, Li D, Hao Y (2017) Tungsten based anisotropic metamaterial as an ultra-broadband absorber. Opt Mater Express 7(2):606–617. https://doi.org/10.1364/OME.7.000606

19. Hoa NTQ, Tung PD, Lam PH, Dung ND, Quang NH (2018) Numerical study of an ultrabroadband, wide-angle,

polarization-insensitivity metamaterial absorber in the visible region. J Electron Mater 47(5):2634–2639

20. Dang PT, Vu TV, Kim J, Park J, Nguyen VC, Vo DD, Nguyen TK, Le KQ, Lee JH (2020) Efficient broadband truncated-pyramid-based metamaterial absorber in the visible and near-infrared regions. Crystals 10(9):784. https://doi.org/10.3390/cryst10090784

21. Hoa NTQ, Lam PH, Tung PD, Tuan TS, Nguyen H (2019) Numerical study of a wide-angle and polarization insensitive ultrabroadband metamaterial absorber in visible and near-infrared region. IEEE Photon J 11(1):4600208. https://doi.org/10.1007/s11664-018-6100-5

22. Liu Y, Liu H, Jin Y, Zhu L (2020) Ultra-broadband perfect absorber utilizing a multi-size rectangular structure in the UV-MIR range. Results Phys 18:103336

23. Yue S, Hou M, Wang R, Guo H, Hou Y, Li M, Zhang Z, Wang Y, Zhang Z (2020) Ultra-broadband metamaterial absorber from ultraviolet to long-wave infrared based on CMOS-compatible materials. Opt Express 28(21):31844–31861. https://doi.org/10.1016/j.rinp.2020.103336

24. Tuan TS, Hoa NTQ (2019) Numerical Study of an Efficient Broadband Metamaterial Absorber in Visible Light Region. IEEE Photonics J 11(3):4600810. https://doi.org/10.1109/JPHOT.2019.2910806

25. Bilal RMH, Baqir MA, Choudhury PK, Naveed MA, Ali MM, Rahim AA (2020) Ultrathin broadband metasurface-based absorber comprised of tungsten nanowires. Results Phys 19:103471. https://doi.org/10.1016/j.rinp.2020.103471

26. Lei L, Li S, Huang H, Tao K, Xu P (2018) Ultra-broadband absorber from visible to near-infrared using plasmonic metamaterial. Opt Express 26(5):5686–5693. https://doi.org/10.1364/OE.26.005686

27. Wu S, Gu Y, Ye Y, Ye H, Chen L (2018) Omnidirectional broadband metasurface absorber operating in visible to near-infrared regime. Opt Express 26(17):21479–21489. https://doi.org/10.1364/OE.26.021479

28. Liu J, Ma WZ, Chen W, Yu GX, Chen YS, Deng XC, Yang CF (2020) Numerical analysis of an ultra-wideband metamaterial absorber with high absorptivity from visible light to near-infrared. Opt Express 28 (16):23748–23760. https://doi.org/10.1364/OE.399198

29. Wu T, Lai J, Wang S, Li X, Huang Y (2017) UV-visible broadband wide-angle polarizationinsensitive absorber based on metal groove structures with multiple depths. Appl Opt 56(21):5844–5848. https://doi.org/10.1364/AO.56.005844

30. Huang Y, Liu L, Pu M, Li X, Ma X, Luo X (2018) Refractory metamaterial absorber for ultra-broadband, omnidirectional and polarization-independent absorption in the UV-NIR spectrum. Nanoscale 10:8298–8303. https://doi.org/10.1039/C8NR01728J

31. Palik ED (1985) Handbook of Optical Constants of Solids. Academic Press, New York, NY, USA

32. Ghosh G (1999) Dispersion-equation coefficients for the refractive index and birefringence of calcite and quartz crystals. Opt Commun 163(1-3):95–102. https://doi.org/10.1016/S0030-4018(99)00091-7

33. Chejarla S, Thummaluru S, Chaudhary R (2018) Flexible metamaterial absorber with wide incident angle insensitivity for conformal applications. Electron Lett 55:133–134

34. Smith DR, Vier DC, Koschny T, Soukoulis CM (2005) Electromagnetic parameter retrieval from inhomogeneous metamaterials. Phys Rev E 71(3):036617. https://doi.org/10.1103/PhysRevE.71.036617

35. Johnson PB, Christy RW (1974) Optical Constants of the Transition Metals. Phys Rev B 9(12):5056. https://doi.org/10.1103/PhysRevB.9.5056

36. Johnson PB, Christy RW (1972) Optical Constants of the Nobel Metals. Phys Rev B 6(12):4370. https://doi.org/10.1103/PhysRevB.6.4370